Mon. Not. R. Astron. Soc. **398,** L26–L30 (2009) doi:10.1111/j.1745-3933.2009.00700.x

Resolving the high redshift Lyα forest in smoothed particle hydrodynamics simulations

James S. Bolton[1]⋆ and George D. Becker[2]

[1]*Max Planck Institut für Astrophysik, Karl-Schwarzschild Str. 1, 85748 Garching, Germany*
[2]*Kavli Institute for Cosmology and Institute of Astronomy, Madingley Road, Cambridge CB3 0HA*

Accepted 2009 June 12. Received 2009 June 12; in original form 2009 April 23

ABSTRACT

We use a large set of cosmological smoothed particle hydrodynamics (SPH) simulations to examine the effect of mass resolution and box size on synthetic Lyα forest spectra at $2 \leq z \leq 5$. The mass resolution requirements for the convergence of the mean Lyα flux and flux power spectrum at $z = 5$ are significantly stricter than at lower redshift. This is because transmission in the high redshift Lyα forest is primarily due to underdense regions in the intergalactic medium (IGM), and these are less well resolved compared to the moderately overdense regions which dominate the Lyα forest opacity at $z \simeq 2$–3. We further find that the gas density distribution in our simulations differs significantly from previous results in the literature at large overdensities ($\Delta > 10$). We conclude that studies of the Lyα forest at $z = 5$ using SPH simulations require a gas particle mass of $M_{\rm gas} \leq 2 \times 10^5\, h^{-1}\, {\rm M}_{\odot}$, which is $\gtrsim$8 times the value required at $z = 2$. A box size of at least $40\, h^{-1}$ Mpc is preferable at all redshifts.

Key words: methods: numerical – intergalactic medium – quasars: absorption lines.

1 INTRODUCTION

Most observations of the Lyα forest are at $2 \leq z \leq 4$; this is where the highest quality optical spectra and the largest data sets are available. Consequently, many studies of hydrodynamical Lyα forest simulations also focus on this redshift range (for a review see Meiksin 2007). The convergence of a variety of simulated Lyα forest statistics with resolution and box size has been explored in detail at $z < 4$, both for Eulerian grid and Lagrangian smoothed particle hydrodynamics (SPH) simulations (Theuns et al. 1998; Bryan et al. 1999; Regan, Haehnelt & Viel 2007). In recent years, however, the importance of the $z \gtrsim 4$ Lyα forest as a probe of the hydrogen reionization epoch (Fan et al. 2006; Becker, Rauch & Sargent 2007) has led to considerable interest in the properties of hydrodynamical Lyα forest simulations at the *highest* observable redshifts (Paschos & Norman 2005; Bolton & Haehnelt 2007).

However, it is not obvious that the numerical requirements for simulating the Lyα forest at $z \gtrsim 4$ are the same as at lower redshifts. The average transmission of the Lyα forest decreases towards higher redshift as the physical gas density increases and the intensity of the ultraviolet (UV) background falls. Absorption lines associated with the mildly overdense regions of the intergalactic medium (IGM) at $z \simeq 2$ are gradually replaced by transmission peaks from underdense regions, culminating in completely saturated absorption by $z \simeq 6$. The decrease in the characteristic overdensity associated with the Lyα forest towards higher redshift will place strong demands on SPH simulations, which naturally focus on resolving high-density regions, as a function of time.

In this Letter, we analyse a large set of cosmological simulations performed with an upgraded version of the SPH code GADGET-2 (Springel 2005). We consider the convergence of two widely used Lyα forest flux statistics, the mean flux and the flux power spectrum, with mass resolution and box size. We also examine the gas density distribution in our simulations in detail. Although some of the issues discussed in this Letter are generally appreciated, there have been no studies of SPH Lyα forest simulations at $z \simeq 5$ where they are highlighted explicitly. Our intention is that these results will provide a useful reference for future modelling of the Lyα forest at the highest observable redshifts.

2 SIMULATIONS

We perform 24 hydrodynamical simulations using GADGET-3, an upgraded version of the publicly available parallel Tree-SPH code GADGET-2 (Springel 2005). The simulations are summarized in Table 1, and cover a wide range of comoving box sizes and gas particle masses. The simulations are all started at $z = 99$, with initial conditions constructed using the same random seed. The cosmological parameters are $(\Omega_{\rm m}, \Omega_{\Lambda}, \Omega_{\rm b}\, h^2, h, \sigma_8, n_{\rm s}) = (0.26, 0.74, 0.024, 0.72, 0.85, 0.95)$. These are consistent with the fifth year *Wilkinson Microwave Anisotropy Probe* (*WMAP*) data (Dunkley et al. 2009) aside from σ_8, which is in better agreement with Lyα

⋆E-mail: jsb@mpa-garching.mpg.de

Table 1. Mass resolution and box size (comoving) of the hydrodynamical simulations used in this work.

Name	L (h^{-1} Mpc)	Total particle number	$M_{\rm gas}$ (h^{-1} M$_\odot$)
2.5–50	2.5	2×50^3	1.61×10^6
2.5–100	2.5	2×100^3	2.01×10^5
2.5–200	2.5	2×200^3	2.51×10^4
2.5–400	2.5	2×400^3	3.14×10^3
5–50	5	2×50^3	1.29×10^7
5–100	5	2×100^3	1.61×10^6
5–200	5	2×200^3	2.01×10^5
5–400	5	2×400^3	2.51×10^4
10–50	10	2×50^3	1.03×10^8
10–100	10	2×100^3	1.29×10^7
10–200	10	2×200^3	1.61×10^6
10–400	10	2×400^3	2.01×10^5
20–50	20	2×50^3	8.22×10^8
20–100	20	2×100^3	1.03×10^8
20–200	20	2×200^3	1.29×10^7
20–400	20	2×400^3	1.61×10^6
40–50	40	2×50^3	6.58×10^9
40–100	40	2×100^3	8.22×10^8
40–200	40	2×200^3	1.03×10^8
40–400	40	2×400^3	1.29×10^7
80–50	80	2×50^3	5.26×10^{10}
80–100	80	2×100^3	6.58×10^9
80–200	80	2×200^3	8.22×10^8
80–400	80	2×400^3	1.03×10^8

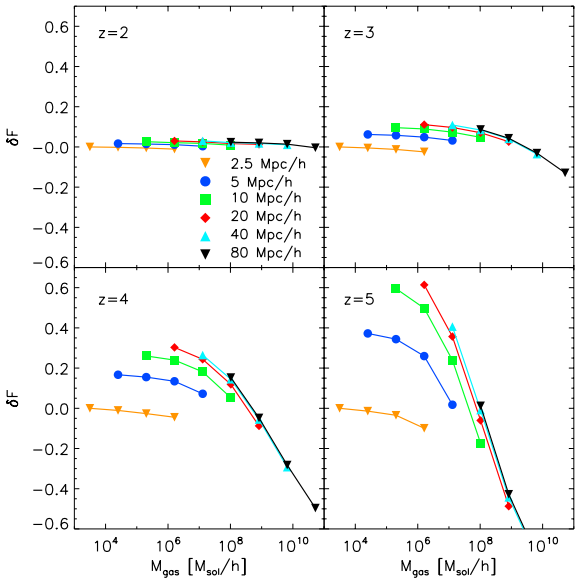

Figure 1. The difference in the mean Lyα flux, $\delta F = (\langle F \rangle - \langle F \rangle_{\rm f})/\langle F \rangle_{\rm f}$ relative to a fiducial value, $\langle F \rangle_{\rm f}$, as a function of gas particle mass for the hydrodynamical simulations listed in Table 1. The four panels display the results at $z = (2, 3, 4, 5)$ where $\langle F \rangle_{\rm f} = (0.843, 0.601, 0.286, 0.072)$, corresponding to the values in the highest resolution simulation (2.5–400). Note, however, this is not necessarily the preferred model due to its small box size. The relative difference becomes significantly larger at higher redshifts for decreasing mass resolution and box size.

forest constraints (Viel, Haehnelt & Springel 2004; Seljak et al. 2005). The gas is assumed to be of primordial composition with a helium mass fraction of $Y = 0.24$. The gravitational softening length is set to 1/30th of the mean linear interparticle spacing. Star formation is included using a simplified prescription which converts all gas particles with overdensity $\Delta = \rho/\langle\rho\rangle > 10^3$ and temperature $T < 10^5$ K into collisionless stars.

The baryons in the simulations are photoionized and heated by the UV background model of Haardt & Madau (2001) which includes emission from both quasars and galaxies. The UV background is switched on at $z = 9$ and is applied in the optically thin limit using a non-equilibrium ionization algorithm. The He II photoheating rate is increased by a factor of 1.8 to give temperatures similar to existing measurements (Schaye et al. 2000). Synthetic Lyα forest spectra are constructed from each simulation at $z = (2, 3, 4, 5)$. Note that in this work we do not subsequently alter the resolution or S/N of the spectra.

3 RESULTS

3.1 Convergence of flux statistics

We first consider the simplest Lyα forest observable, the mean flux, $\langle F \rangle = \langle e^{-\tau} \rangle$, in Fig. 1. This shows the difference in $\langle F \rangle$ measured from our synthetic spectra relative to the highest resolution model (2.5–400) as a function of gas particle mass at $z = (2, 3, 4, 5)$. At $z = 2$, the mean flux converges quickly with mass resolution. There is a 0.5 (1.3) per cent different between the 20–200 (20–100) and 20–400 models, giving a good degree of convergence with resolution for $M_{\rm gas} = 1.61 \times 10^6\, h^{-1}\,{\rm M}_\odot$. Convergence of $\langle F \rangle$ with box size may be judged by the vertical separation between data points with the same gas particle mass. A 20 h^{-1} Mpc box provides acceptable results at $z = 2$, with a 0.7 (0.2) per cent difference between the 20–100 (40–200) and 80–400 models. Tytler et al. (2009), who recently examined the convergence of $\langle F \rangle$ with box size at $z = 2$ using the Eulerian hydrodynamical code ENZO, find similar results.

However, it is clear that the relative difference becomes significantly larger with increasing redshift and decreasing mass resolution. By $z = 5$, there is a 2.1 (8.2) per cent difference between $\langle F \rangle$ in the 5–200 (5–100) and 5–400 models. Only a marginal degree of convergence with mass resolution is achieved for $M_{\rm gas} = 2.01 \times 10^5\, h^{-1}\,{\rm M}_\odot$. The differences due to box size also become larger, with a 7.2 (2.1) per cent difference between $\langle F \rangle$ in the 20–100 (40–200) and 80–400 models. Clearly, the box size and mass resolution requirements for simulating the mean flux of the Lyα forest are much stricter at higher redshift.

The second statistic we consider is the 1D Lyα flux power spectrum. This has been extensively used as a probe of the primordial matter power spectrum on scales of 0.5–40 h^{-1} Mpc at $2 \leq z \leq 4$, and there are several studies which examine its convergence with resolution and box size in some detail (McDonald 2003; Viel et al. 2004). There has been comparatively little work performed at higher redshifts (but see Viel et al. 2008). The upper panels in Fig. 2 display the power spectrum of the Lyα flux, $F = e^{-\tau}$, at $z = 2$ and $z = 5$ computed from the simulations with a box size of 10 h^{-1} Mpc. The vertical dotted lines bracket the range of wavenumbers used by Viel et al. (2004) to infer the amplitude and shape of the matter power spectrum at $z < 3$. Note that we have rescaled the synthetic spectra to have the same $\langle F \rangle$ for this comparison. The convergence with mass resolution is again significantly poorer at $z = 5$ and is also scale dependent. For the range $0.003 < k\,[{\rm s\,km^{-1}}] < 0.03$ at $z = 2$, the 10–200 (10–100) data are within 1 (3) per cent of the 10–400 model, corresponding to a requirement for $M_{\rm gas} = 1.61 \times 10^6\, h^{-1}\,{\rm M}_\odot$. However, at $z = 5$, the 10–200 (10–100) model deviates from 10–400 by to 7 (22) per cent, while the 5–200 (5–100) simulations (not shown) deviate from 5–400 by 2 (6) per cent. A

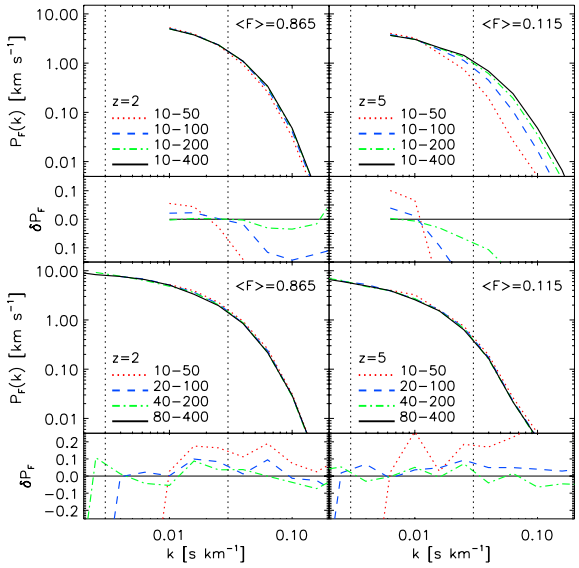

Figure 2. The upper panels show the 1D flux power spectrum computed from simulations with fixed box size ($10\,h^{-1}$ Mpc) at $z = 2$ and 5, while the lower panels display the power spectrum from simulations with fixed mass resolution ($1.03 \times 10^8\,h^{-1}\,\mathrm{M}_\odot$). The spectra have been rescaled to have the same mean flux, indicated in the upper right of each panel. The difference in the power spectrum relative to the models represented by the solid curves is shown in the lower third of each panel. The vertical dotted lines bracket the range of wavenumbers used by Viel et al. (2004) to infer the amplitude and shape of the matter power spectrum, $0.003 < k\,[\mathrm{s\,km^{-1}}] < 0.03$.

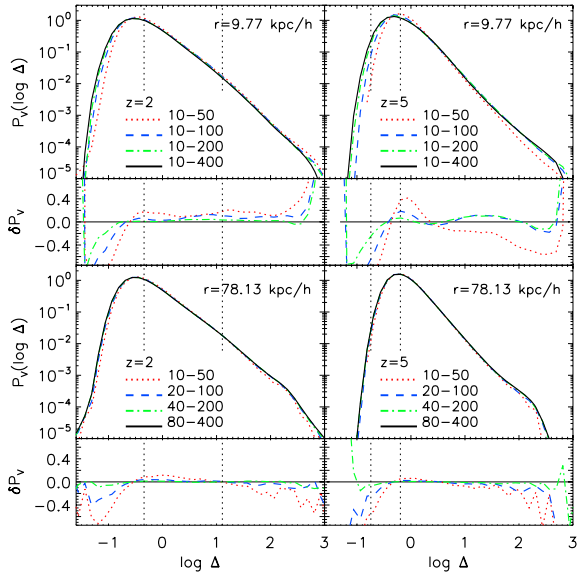

Figure 3. The upper panels show the volume weighted gas density distribution computed from simulations with fixed box size ($10\,h^{-1}$ Mpc) at $z = 2$ and 5, while the lower panels display the density distribution from simulations with fixed mass resolution ($1.03 \times 10^8\,h^{-1}\,\mathrm{M}_\odot$). The difference in the density distribution relative to the models represented by the solid curves is shown in the lower third of each panel. The vertical dotted lines in each panel bracket the range of optical depth weighted overdensities corresponding to 95 per cent of all the pixels with $0.05 \le F \le 0.95$ in the associated Lyα forest spectra.

mass resolution of at least $M_{\rm gas} = 2.01 \times 10^5\,h^{-1}\,\mathrm{M}_\odot$ is required at $z = 5$ for marginal convergence.

The lower panels in Fig. 2 display the effect of box size on $P_{\rm F}(k)$ for fixed mass resolution. At $z = 5$, the 20–100 (40–200) model is within 10 (8) per cent of the 80–400 model, while at $z = 2$ the 20–100 (40–200) model is within 10 (9) per cent of the 80–400 model. A box size of at least $40\,h^{-1}$ Mpc is therefore required to adequately model the power spectrum at $2 \le z \le 5$. Similar requirements have been noted by McDonald (2003) and Viel et al. (2004) at $z \simeq 2$–3. We also performed an examination of a third flux statistic, the distribution of the Lyα flux. We again found the simulation requirements to be significantly stricter towards higher redshifts, with the same box size and resolution requirements as the mean flux. We do not report these results in detail here.

3.2 The gas density distribution

The explanation for these results is apparent on inspecting the gas density distribution in the simulations. The upper panels in Fig. 3 display the volume weighted density distribution per unit $\log\Delta$ at $z = 2$ and 5 for models with a box size of $10\,h^{-1}$ Mpc, while the lower panels display the results for fixed mass resolution. The density distributions are obtained by interpolating the particle masses, weighted by the smoothing kernel, on to a regular grid with a cell size, r, indicated in each panel. The vertical dotted lines in each panel bracket the range of optical depth weighted overdensities corresponding to 95 per cent of all the pixels with $0.05 \le F \le 0.95$ in the associated Lyα forest spectra. The mean flux of the spectra at $z = (2, 5)$ is $\langle F\rangle = (0.865, 0.115)$.

At $z = 2$, the 10–200 (10–100) density distribution is within 5 (13) per cent of the 10–400 model for $-0.5 \le \log\Delta \le 2.5$, while at $z = 5$ the 10–200 (10–100) is within 12 (18) per cent of 10–400, providing at best marginal convergence. Outwith this density range, the distribution has not converged at either redshift. In the lower two panels, the 40–200 (20–100) is within 3 (12) per cent of 80–400 at $z = 2$, and 7 (18) per cent at $z = 5$. It is the poor convergence with mass resolution and box size in the most underdense regions ($\log\Delta < -0.5$) which drives the Lyα forest results. At $z = 2$, the Lyα forest is dominated by gas with $\Delta > 1$. The transmission from underdense regions is always close to the continuum ($F = 1$) regardless of mass resolution, and so under-resolving these regions has little impact on the Lyα flux statistics. In contrast, underdense regions dominate the transmission at $z = 5$, impacting significantly on the convergence of the simulated Lyα forest properties.

This behaviour is a consequence of the spatially adaptive nature of SPH, which provides excellent spatial resolution in high-density regions but poorer resolution in underdense regions. In Fig. 4, we

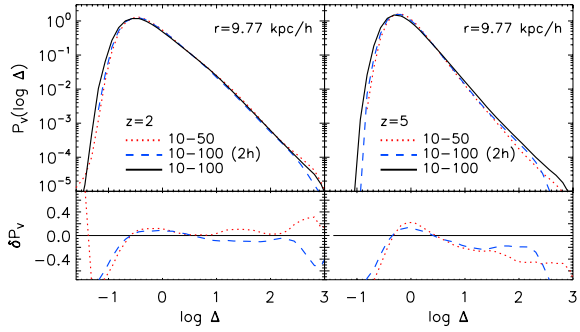

Figure 4. The volume weighted gas density distribution at $z = 2$ (left-hand panel) and $z = 5$ (right-hand panel) from the 10–50 (dotted curve) and 10–100 (solid curve) models. The dashed curve is computed from the 10–100 simulation after doubling the particle smoothing lengths, matching those used in the 10–50 model in order to mimic lower mass resolution.

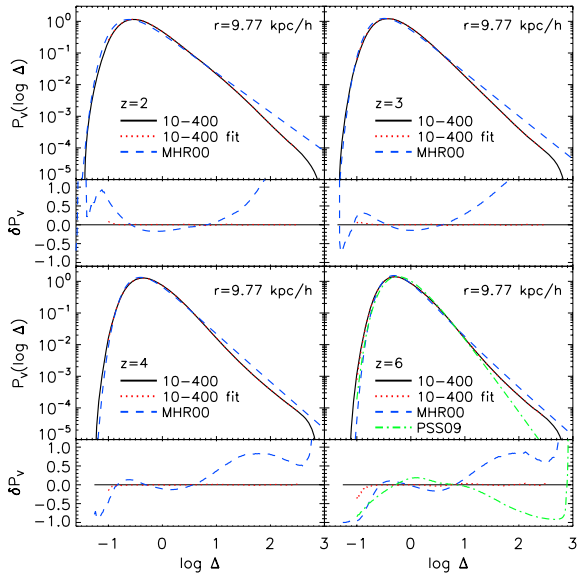

Figure 5. The volume weighted gas density distribution extracted from the 10–400 simulation at $z = (2, 3, 4, 6)$ (solid curves). The dotted curves correspond to an eighth-order polynomial fit to the simulation data over the range $-1 \leq \log \Delta \leq 2.5$. The fits obtained by MHR00 correspond to the dashed curves. The dot–dashed curve in the panel at $z = 6$ also shows the recent fit presented by PSS09. The differences in the fits relative to the simulation data are shown in the lower third of each panel.

demonstrate this by comparing the density distribution from the 10–50 and 10–100 models to a third distribution, again drawn from the 10–100 model. The latter is computed by interpolating the particle masses on to a grid using the 10–50 model particle smoothing lengths (twice the 10–100 values), mimicking particle masses a factor of eight larger. The 10–50 distribution at low densities is well reproduced by the resmoothed 10–100 distribution, implying that differences in the density distribution at $\log \Delta < -0.5$ are largely a consequence of the intrinsic mass resolution limit. However, additional effects such as gas being transferred from the low density IGM to previously unresolved haloes may also play a small role (Theuns et al. 1998).

Lastly, we consider fits to the gas density distribution which are widely used in analytical models of the Lyα forest. In Fig. 5, we compare the volume weighted density distribution from our 10–400 simulation to the four parameter fits[1] obtained at $z = (2, 3, 4)$ by Miralda-Escudé, Haehnelt & Rees (2000, hereafter MHR00). The solid curves in Fig. 5 correspond to our 10–400 simulation data, while the dashed curves show the fits obtained by MHR00. The dot–dashed curve at $z = 6$ corresponds to a more recent fit[2] to an SPH simulation by Pawlik, Schaye & van Scherpenzeel (2009, hereafter PSS09), who also use the parametrization suggested by MHR00.

Although our simulation is in reasonable agreement with the MHR00 fits for $-0.5 \leq \log \Delta \leq 1$, we confirm the claim by PSS09 that the power-law tail in the MHR00 parametrization, $P_{\rm V}(\Delta) \propto \Delta^{-\beta}$ for $\Delta \gg 1$, provides a poor description of the density distribution. This is perhaps not too surprising; the MHR00 prescription is based on the assumption of a power-law density profile for collapsed objects and is not obtained directly from the simulations. The 10–400 model also differs considerably from the MHR00 fits at $\log \Delta < -0.5$, although note that our data are not fully converged here. The PSS09 fit is in poor agreement with our simulation at $z = 6$. However, PSS09 find a similar discrepancy between their fit and simulation results, suggesting that the difference between their *simulated* density distribution and our data is actually much smaller. Furthermore, we use a very different star formation prescription to PSS09 which is designed to optimize Lyα forest simulations. We have verified this has little effect on the simulated gas density distribution at $\log \Delta < 2$ when compared to a more sophisticated star formation prescription (Springel & Hernquist 2003), but this choice will produce differences in the density distribution at higher densities.

We conclude that the MHR00 parametrization is not fully adequate for describing $P_{\rm V}$ from our simulations at $\log \Delta > 1$. Consequently, we provide polynomial fits to the 10–400 density distribution in Table 2 over the range $-1 \leq \log \Delta \leq 2.5$ *only* (dotted curves in Fig. 5). We deliberately avoid parametrizing the data, preferring to instead provide an accurate representation of the simulations for reference. Note, however, that $P_{\rm V}$ is still only marginally converged with resolution for $-0.5 \leq \log \Delta \leq 2.5$ and has not fully converged with box size.

4 CONCLUSIONS

We perform a large set of cosmological SPH simulations to explore the effect of mass resolution and box size on two key Lyα forest flux statistics. As noted in many previous studies (see Meiksin 2007 for a review), we find a mass resolution of $M_{\rm gas} = 1.61 \times 10^6\, h^{-1}\, {\rm M}_\odot$ is more than adequate for simulating mean Lyα flux and power spectrum at $z = 2$. However, towards higher redshift the mass resolution requirement for convergence becomes significantly stricter, with a gas particle mass *at least* 8 times smaller required at $z = 5$. We demonstrate this is largely a consequence of the intrinsic resolution limit of SPH simulations in low-density regions. Although a $20\, h^{-1}$ Mpc box is adequate for simulating the mean flux at $z = 2$, a $40\, h^{-1}$ Mpc box is required for the power spectrum, and this is preferred for both statistics at $z = 5$. We also briefly demonstrate that the MHR00 parametrization for the gas density distribution, although in reasonable agreement with our 10–400 model at moderate overdensities, provides a poor description of the simulation for $\Delta > 10$.

Although our results will hold in general for SPH Lyα forest simulations, in detail they will only be exact for the specific models we present. Convergence requirements will always depend on the physical process under consideration, as well as the precision of the observational data to which the simulations are compared. We have also assumed that the $z \gtrsim 5$ forest is dominated by transmission from underdense regions in the IGM. This picture is correct if the UV background is spatially uniform, but if there are large fluctuations in the ionising radiation field at $z \gtrsim 5$, localized patches of highly ionized gas will complicate this interpretation somewhat. Lastly, at lower redshifts where the Lyα forest transmission is dominated by mildly overdense regions, SPH simulations produce results comparable to those from state-of-the-art adaptive mesh codes (Regan et al. 2007). It would be very interesting to perform a similar comparison at $z \simeq 5$.

[1] The MHR00 fits are derived from the L10 simulation of Miralda-Escudé et al. (1996), which uses $(\Omega_{\rm m}, \Omega_\Lambda, \Omega_{\rm b}\, h^2, h, \sigma_8, n_{\rm s}) = (0.4, 0.6, 0.015, 0.65, 0.79, 0.96)$, with a box size of $10\, h^{-1}$ Mpc and 288^3 cells. This gives an average gas mass per cell of $6 \times 10^5\, {\rm M}_\odot$. Note that the $z = 6$ MHR00 distribution is an extrapolation from the lower redshift fits.

[2] PSS09 use a GADGET-2 simulation with $(\Omega_{\rm m}, \Omega_\Lambda, \Omega_{\rm b}\, h^2, h, \sigma_8, n_{\rm s}) = (0.258, 0.742, 0.0228, 0.719, 0.796, 0.963)$, a box size of $6.25\, h^{-1}$ Mpc and $M_{\rm gas} = 1.8 \times 10^5\, h^{-1}\, {\rm M}_\odot$ (256^3 gas particles).

Table 2. Tabulated coefficients for the eighth-order polynomial fits to the gas density distribution from our 10-400 simulation, $\log[P_V(x)] = \sum_i a_i x^i$, where $x = \log\Delta$. $P_V(\Delta)$ is normalized to unity and $\Delta P_V(\Delta) = P(\log\Delta)/\ln 10$. Note that the fits are made over the range $-1 \leq \log\Delta \leq 2.5$ *only*, and are all within <5 per cent of the simulation data for $-0.5 \leq \log\Delta \leq 2.5$.

z	a_0	a_1	a_2	a_3	a_4	a_5	a_6	a_7	a_8
7.0	−0.038744	−1.193136	−1.209168	1.480778	−1.355202	0.649847	−0.093190	−0.024297	0.006604
6.5	−0.045600	−1.162781	−1.187344	1.312205	−1.225248	0.647885	−0.120218	−0.014682	0.005503
6.0	−0.059247	−1.148617	−1.122149	1.176996	−1.178106	0.661365	−0.105707	−0.031420	0.008956
5.5	−0.077189	−1.115055	−1.049649	0.913821	−1.018321	0.774770	−0.259515	0.025978	0.001650
5.0	−0.089459	−1.083824	−1.051325	0.669231	−0.709611	0.777568	−0.414747	0.101665	−0.009361
4.5	−0.102984	−1.100786	−1.064773	0.677866	−0.542385	0.556266	−0.298218	0.072713	−0.006496
4.0	−0.132602	−1.132429	−0.970648	0.719472	−0.552924	0.418740	−0.169566	0.029132	−0.001301
3.5	−0.163770	−1.134785	−0.885486	0.611691	−0.404073	0.374816	−0.230005	0.070230	−0.008295
3.0	−0.203625	−1.166205	−0.784556	0.642483	−0.324878	0.199731	−0.147317	0.059290	−0.008639
2.5	−0.259451	−1.190049	−0.614461	0.661790	−0.367005	0.090334	−0.034647	0.021446	−0.004244
2.0	−0.325057	−1.184408	−0.442799	0.566567	−0.347644	0.074473	−0.016128	0.012290	−0.002695

ACKNOWLEDGMENTS

We thank M.G. Haehnelt, M. McQuinn, S.P. Oh, J. Pritchard, V. Springel and M. Viel for valuable comments. The simulations used in this work were performed using the COSMOS facility at DAMTP in Cambridge. COSMOS is sponsored by SGI, Intel, HEFCE and STFC. GDB acknowledges financial support from the Kavli foundation.

REFERENCES

Becker G. D., Rauch M., Sargent W. L. W., 2007, ApJ, 662, 72
Bolton J. S., Haehnelt M. G., 2007, MNRAS, 382, 325
Bryan G. L., Machacek M., Anninos P., Norman M. L., 1999, ApJ, 517, 13
Dunkley J. et al., 2009, ApJS, 180, 306
Fan X. et al., 2006, AJ, 131, 1203
Haardt F., Madau P., 2001, in Neumann D. M., Tran J. T. V., eds, Clusters of Galaxies and the High Redshift Universe Observed in X-rays. preprint (astro-ph/0106018)
McDonald P., 2003, ApJ, 585, 34
Meiksin A. A., 2007, preprint (arXiv:0711.3358)
Miralda-Escudé J., Cen R., Ostriker J. P., Rauch M., 1996, ApJ, 471, 582
Miralda-Escudé J., Haehnelt M., Rees M. J., 2000, ApJ, 530, 1 (MHR00)
Paschos P., Norman M. L., 2005, ApJ, 631, 59
Pawlik A. H., Schaye J., van Scherpenzeel E., 2009, MNRAS, 394, 1812 (PSS09)
Regan J. A., Haehnelt M. G., Viel M., 2007, MNRAS, 374, 196
Schaye J., Theuns T., Rauch M., Efstathiou G., Sargent W. L. W., 2000, MNRAS, 318, 817
Seljak U. et al., 2005, Phys. Rev. D, 71, 103515
Springel V., Hernquist L., 2003, MNRAS, 339, 289
Springel V., 2005, MNRAS, 364, 1105
Theuns T., Leonard A., Efstathiou G., Pearce F. R., Thomas P. A., 1998, MNRAS, 301, 478
Tytler D., Paschos P., Kirkman D., Norman M. L., Jena T., 2009, MNRAS, 393, 723
Viel M., Haehnelt M. G., Springel V., 2004, MNRAS, 354, 684
Viel M., Becker G. D., Bolton J. S., Haehnelt M. G., Rauch M., Sargent W. L. W., 2008, Phys. Rev. Lett., 100, 041304

This paper has been typeset from a TEX/LATEX file prepared by the author.